

# An electrical circuit model of chemoreceptor cells based on adaptation and disadaptation time constants: implications for temporal filtering

Paul A. Moore<sup>\*</sup>, Kun Shao

*Laboratory for Sensory Ecology and Center for Neuroscience, Mind, and Behavior, Department of Biological Sciences, Bowling Green State University, Bowling Green, OH 43403, USA*

Received 25 January 1999; received in revised form 25 October 1999; accepted 17 November 1999

## Abstract

Chemoreceptor cells have temporally dynamic physiological properties that serve as filters for fluctuating odor patterns. A computational model, based on an electrical circuit, of a peripheral chemoreceptor cell was developed based on two time constants ( $\tau_1$  and  $\tau_2$ ) that model sensory adaptation and recovery from adaptation. With  $\tau_1$  set to 0.1 s and  $\tau_2$  to 3.8 s, our model receptor cell responded like real olfactory cells when presented with a series of odor pulse trains. As in real olfactory cells, changes in response magnitude and frequency filtering were observed with changes in stimulation frequency. When presented with chaotic stimulus patterns, model receptor cells responded with brief periods of current flow and adapted quickly. Decreases in the first time constant ( $\tau_1$ ) decreased the response magnitude, while decreases in the second time constant ( $\tau_2$ ) increased the response magnitude and pulse frequency resolution during chaotic odor stimulation. The two time constants are important for determining different filter properties of the chemoreceptor cells and define the temporal range of chemical fluctuations to which a single cell will respond. © 2000 Elsevier Science S.A. All rights reserved.

*Keywords:* Chemoreception; Computer model; Odor plumes; Sensory adaptation

## 1. Introduction

Chemical signals are composed of four different components that have potential information about the environment: quality, intensity, spatial, and temporal distributions [1]. The majority of the research that is currently being performed in chemical senses is designed to answer questions on how chemosensory systems function to extract quality and intensity information from chemical signals. A minority of laboratories (Breer, Firestein, and Zufall at the cellular level; Atema, Christensen, and Kaissling at the physiological level) are performing experiments that are explicitly examining questions about spatial and temporal information. As a whole, the understanding of how

chemosensory systems function to extract information from realistic environmental signals is not as complete as other sensory systems such as vision and audition. This is due to two reasons. First, there is a general lack of knowledge and understanding of the spatial and temporal dynamics of odor signals that are perceived and potentially processed by a chemosensory system. Second, because of the physics associated with the dispersion of chemical signals at macroscopic scales, it is impossible to manufacture replicated presentations of environmentally relevant odor signals within either physiological or behavioral testing areas. This second fact constrains the type of questions that can be answered using direct experimentation.

The spatial, temporal, and intensity components of an environmental odor signal are directly due to the physics of chemical dispersion within a moving fluid whether it be air or water. At macroscopic scales, chemical signals are dispersed by turbulence, which results in a patchy signal in time and space [3,20,23,25]. Turbulence is produced by the mechanical forces acting within a moving fluid. Since the

<sup>\*</sup> Corresponding author. Tel.: +1-419-372-8556; fax: +1-419-372-2024.

*E-mail address:* pmoore@bgnnet.bgsu.edu (P.A. Moore).

generation of turbulence is a chaotic phenomenon, each odor signal will have a unique spatial, temporal, and intensity component even under conditions that appear to be similar or identical (For review see [34]). Although theoretically possible, it is currently technologically impossible to replicate the chaotic nature of turbulent odor signals except by the indirect means of electronic playback within computers.

The purpose of this study was to investigate how the physiological properties of peripheral chemosensory cells function to extract temporal, spatial, and intensity information under real environmental stimulus conditions, i.e., turbulent odor plumes. The ideal approach to answering this question would be to determine a number of physiological properties of single sensory cells and then stimulate each single cell with an identical turbulent odor plume. This experimental approach is not possible because the fine-scale control of turbulent stimulus profiles within any testing situation is technologically impossible, as stated above. The only current method available to answer this question is through the use of computational models. The model then serves a purpose of providing insight into the function properties of chemoreceptor cells where physiological experiments are impossible.

Extracting spatial and temporal information from odor signals is an important component to the functioning of many different chemosensory systems. For many terrestrial and aquatic animals, this information is critical for orientation to odor sources. Lobsters and blue crabs, for example, directly use the spatial distribution of odors for directional information during food location [22,33]. In many moth species, the presence or absence of a pheromone will cause the moth to switch between two different orientation strategies [17,29,30]. Odor plumes in both terrestrial and aquatic environments are turbulent, which results in a highly heterogeneous and chaotic signal [21,24,25]. The heterogeneity in odor signals has been shown to be a critical factor for terrestrial insects to maneuver upwind. In wind tunnel experiments, moths exposed to continuously released or homogeneous pheromone plumes will not fly upwind [15], while moths exposed to large turbulent plumes or high frequency pulsed plumes located the source of the odor [4].

In all of these examples, the temporal structure of signals within turbulent odor plumes either guides the switch between orientation strategies (moths) or provides directional information (crustaceans). Understanding the extraction of information from temporally heterogeneous signals by the chemosensory system is crucial to understanding both orientation in detail and the evolution of physiological properties of chemosensory systems. The extraction of temporal information from odor plumes depends upon the temporal properties of chemoreceptor cells (adaptation and disadaptation). Constant stimulation will lead to receptor adaptation, which may explain the loss of upwind movement in moths [4,30]. A dynamic balance between stimulus structure and receptor cell properties will

likely give the best sensitivity for the tracking of odor plumes.

Studies of the temporal properties of chemoreceptors have focused on pulse frequency resolution [2,6,10–12,14,26], adaptation and disadaptation rates [31], dynamic changes in receptor threshold [5], and changes in generator potential [18]. These studies coupled with knowledge of natural stimulus patterns have led to a series of models that have begun to provide us with an understanding of temporal filtering in chemosensory systems [19,20]. These adaptation and disadaptation processes have been modeled as a dynamic change of response threshold [19,20]. Such models separate adaptation and disadaptation into two distinct and independent time constants. In addition, recent models have segregated chemoreceptor cells into two distinct types of detectors: flux detectors and concentration detectors [13]. This distinction is critical for understanding how these two types of detectors encode the temporally heterogeneous chemical signal.

Recently, investigators conducted a series of experiments designed to quantitatively study the adaptation and disadaptation properties of peripheral chemoreceptor cells in the lobster [12]. These experiments were unique in that they directly measured stimulus concentration and temporal profiles during neurophysiological recordings. These simultaneous measures of stimulus input and receptor output provided some of the most detailed measurements of the temporal properties of chemoreceptor cells to date. We have used the results of these studies in an electrical circuit model of peripheral chemoreceptor cells. This model is an extension of classical theoretical modeling developed initially by Lopicque [16] and was called the leaky integrator model. Basically, an electrical circuit models the neuron with a capacitor in parallel with a resistor and battery. We chose this type of model to answer questions concerning the functional role that adaptation and disadaptation play in filtering turbulent odor signals. We have purposefully drawn a “black box” around the cellular mechanisms underlying these processes because we are primarily concerned with the functional consequences of adaptation and disadaptation. In addition, the benefit of this type of model is that solving these equations leads only to first-order differential equations and that we can examine input–output relationships of the neuron. In our model, the two time constants associated with adaptation and disadaptation are assigned to two distinct processes; the charging and restoring processes in a capacitor–resistor circuit.

As stated above, modeling has a distinct advantage over direct experimentation due to the technical difficulty of measuring the temporal properties of olfactory cells and then presenting these cells with temporally dynamic stimuli that are environmentally relevant. This approach allows the investigator to repeatedly stimulate receptor cells that have different physiological properties with the identical turbulent odor signals. This can lead to new insights into how individual or population of cells serves to encode the

many potential sources of information, such as intensity, quality, spatial or temporal information, from complex natural stimuli.

## 2. Materials and methods

### 2.1. General circuit model equations

We have developed a model to investigate the functional responses of peripheral chemoreceptor cells. This model is not designed to be physiologically equivalent to a real receptor cell, but is simply designed to have similar input–output relationships. To model the input–output relationship of a chemoreceptor cell, we have adopted the Lapicque model for a neuron. The neuron can be modeled by an electrical RC (Resistor–Capacitor) circuit (Fig. 1). The mathematics follows Eccles [8], Curtis and Eccles [7], and Tuckwell [28]. Stimulus input is modeled by a voltage input ( $V_{in}$ ) to the model receptor cell. In addition, the response is represented by current flow ( $I$ ) in our model. The response of the model cell is then determined by Ohm's law (1):

$$I = (V_{in} - V)/R \quad (1)$$

where the output of the model cell is determined by the voltage difference between the stimulus input ( $V_{in}$ ) and the voltage charge on the capacitor ( $V$ ). We assume that there are two processes, charging and restoring, that determine the voltage on the capacitor of the model cell. These two processes interact to adapt a model cell to an input signal  $V_{in}$ , while only the restoring process disadapts the model cell after removal of the stimulus.

#### 2.1.1. Adaptation

The physiological responses of chemoreceptor cells often return to pre-stimulus levels in spite of continual stimulation. This process, termed adaptation, can be thought of as a dynamic change in the response threshold of the receptor cell [5,14]. Atema and co-workers have shown in lobster chemoreceptor cells that the response of the receptor cell decays exponentially [10–12,31]. When a constant

stimulus ( $V_{in}$ ) is applied to the model receptor cell, the capacitor charges and the voltage ( $V$ ) on the capacitor builds up exponentially over time ( $t$ ), ( $dV/dt = I/C$ ; [27]). The voltage difference between input and capacitor ( $V_{in} - V$ ) will decrease and the response of the model receptor cell will decrease exponentially.

We assumed during both the charging and restoring phases that the restoring force serves to work against the voltage change on capacitor ( $dV/dt$ ), i.e., when the voltage rises, the restoring force will decrease  $V$ ; conversely, when the voltage drops, the restoring force will increase  $V$ . In addition, the strength of the restoring force is voltage dependent, i.e., the larger the voltage, the stronger the effect that the restoring force will have on this change. This can be described by the differential Eq. (2):

$$dV/dt = -pV \quad (2)$$

where  $p$  is a constant coefficient and is dependent upon individual cell properties. For convenience, we define the reciprocal of the time constant  $\tau_2$  as equal to  $p$ . Eq. (2) now becomes Eq. (3):

$$dV/dt = -V/\tau_2 \quad (3)$$

In general, the change of voltage on the capacitor over time ( $dV/dt$ ) during adaptation is due to both a positive charging force and a negative restoring force. These two processes are additive and can be modeled by Eq. (4):

$$dV/dt = I/C - V/\tau_2 \quad (4)$$

where  $\tau_2 = CR'$ , the capacitance and resistance of the cell (Fig. 1; [28]).

#### 2.1.2. Disadaptation

When there is no stimulation ( $V_{in} = 0$ ) or stimulation is lower than capacitor voltage ( $V_{in} < V$ ), there will be no positive current flow from the model cell due to the presence of the diode (Fig. 1). The restoring force works to return the voltage on the capacitor to the pre-stimulus level (disadaptation). Since there is no response from the model cell ( $I = 0$ ), Eq. (4) now becomes Eq. (5):

$$dV/dt = -V/\tau_2 \quad (5)$$

#### 2.1.3. Response of the model to a DC stimulus input

We can begin testing our model by presenting the model receptor cell with a DC stimulation, such that when  $t < 0$ ,  $V_{in} = 0$  and when  $t \geq 0$ ,  $V_{in} = V_{DC}$ .  $V_{DC}$  is the voltage of the DC input and is equivalent to the stimulus intensity delivered to the model cell. The response of the model can be calculated by Eqs. (1) and (4) by substituting  $V_{DC}$  for  $V_{in}$ . The solutions for these equations are:

$$I = I_b + k_{DC} \exp(-t/\tau) \quad (6)$$

$$V = Rk_{DC} - Rk_{DC} \exp(-t/\tau) \quad (7)$$

$I_b$  is the basal level of current flow in the model cell or background activity.  $k_{DC}$  is a constant coefficient deter-

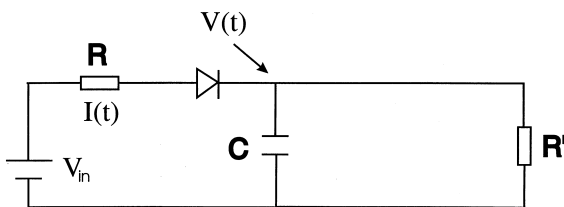


Fig. 1. Electric circuit model of a chemoreceptor cell taken from Lapicque [16] and Eccles [8] and designed to simulate the effects of adaptation and disadaptation on the firing abilities of cells. For the purposes of the model, electrical current ( $I$ ) is analogous to receptor cell output (as changes in firing frequency) and voltage input ( $V_{in}$ ) is analogous to stimulus concentration.

mined by the boundary conditions ( $t = 0, V = 0, I \neq 0$ ), therefore,  $k_{DC} = k_1, I = V_{DC}/R = I_b + k_{DC}$ . In addition,  $I_b, \tau, \tau_1$ , and  $k_1$  are defined as:

$$I_b = (\tau/\tau_2)(V_{in}/R) \quad (8)$$

$$\tau = (\tau_1\tau_2)(\tau_1 + \tau_2) \quad (9)$$

$$\tau_1 = (RC) \quad (10)$$

$$k_1 = (\tau/\tau_1)(V_{in}/R) = (V_{in}/R) - I_b \quad (11)$$

The  $\tau_1, \tau_2$ , and hence,  $\tau$  are intrinsic values of the temporal properties of a specific model receptor cell and are independent of input signal qualities.  $\tau_1$  is determined by the values of  $R$  and  $C$  and is called the ‘‘charging time constant’’ of the model receptor cell.  $\tau_2$  is an intrinsic property of restoring force and is called the ‘‘disadaptation time constant’’.  $\tau$  is the time constant determined by the simultaneous charging and restoring processes and is called ‘‘adaptation time constant’’.

The voltage on the capacitor at the time of initial stimulation is zero, i.e.,  $V_{t=0} = 0$ . We can put our solution for  $k_{DC}$  into Eqs. 6 and 7. From these equations, it becomes possible to calculate both the voltage on the capacitor and the response of the model receptor cell during the DC stimulation. As time increases, the voltage on the capacitor increases exponentially to a value of  $Rk_1$

( $= (\tau/\tau_1)V_{DC}$ ) and the response decreases exponentially to a value of  $I_b$  ( $= (\tau/\tau_2)(V_{DC}/R)$ ).

After removing the DC stimulus, the voltage on the capacitor begins to discharge, which initiates the disadaptation process. The general solution of the differential equation for disadaptation (5) is:

$$V = V_{dis} \exp(-t/\tau_2) \quad (12)$$

where  $V_{dis}$  stands for the voltage at the initial part of the disadaptation phase ( $t = 0$ ) which is  $Rk_1$  (from Eq. (7)), i.e.,

$$V_{dis} = Rk_1 \quad (13)$$

Substituting Eq. 13 into Eq. 12 supplies the equation for the disadaptation phase of the model cell’s response:

$$V = Rk_1 \exp(-t/\tau_2) \quad (14)$$

The voltage on the capacitor decreases exponentially with time. The response on the next stimulation will then depend upon the intensity of the next stimulation and the remnant voltage on the capacitor.

#### 2.1.4. Responses to a repetitive pulse train input

For a series of periodic stimuli with frequency ( $f$ ), the pulse train can be divided into two intervals: one stimulus interval ( $ST_x =$  stimulus period  $x$ ) during the presence of the stimuli ( $V_{in}$ ) and the other stimulus interval ( $IST_x =$

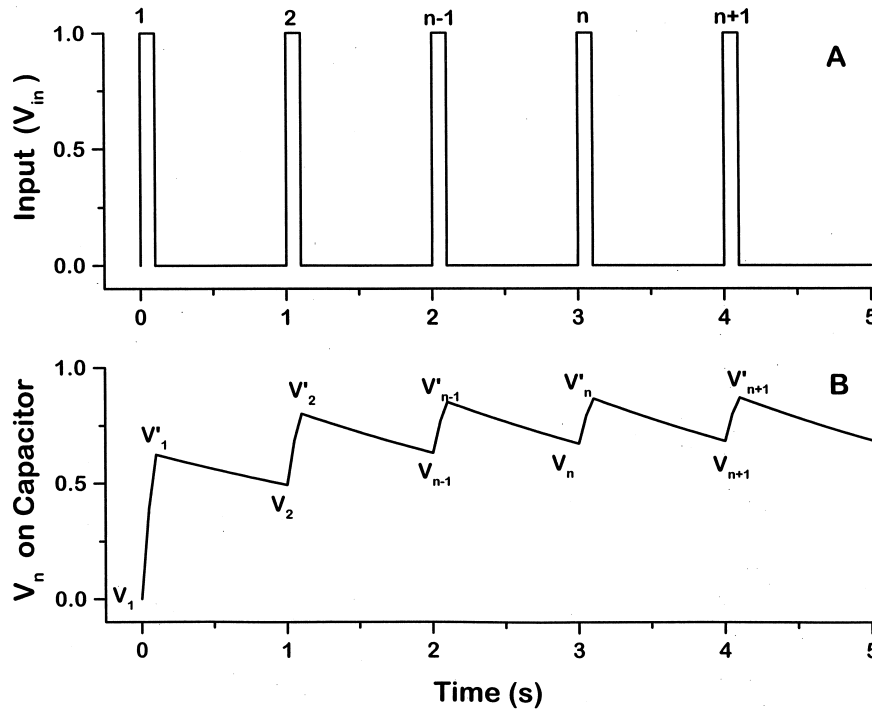


Fig. 2. (A) The periodic stimulus for the model chemoreceptor cell. The total period of the stimulation is  $T = ST_1 + IST_1$  and the frequency of the input is  $1/T$ . (B) Voltage on the capacitor ( $V$ ) changes due to changes in the stimulus input. During the stimulation phase of the periodic stimulus ( $ST$ ), the capacitor charges, while during the inter-stimulus period ( $IST$ ), the capacitor discharges. The rate of charging and discharging are determined by ( $\tau_1$ ) and ( $\tau_2$ ), which are defined in the text. The time constants are set at 0.1 and 3.8 s for  $\tau_1$  and  $\tau_2$  for all analysis except where explicitly stated.

inter-stimulus period  $x$ ), which is between successive stimuli ( $V_{in} = 0$ ). The total period of the stimuli ( $T$ ) is the summation of both of these intervals (Fig. 2A).

In the first period of stimulation ( $ST_1$ ), the voltage on the capacitor and the response are identical to those derived from the DC stimulation (Fig. 2B,  $V_1 = 0$ ). Eqs. 6 and 7 describe the response (6) and voltage (7) of the model.

At the beginning of the first inter-stimulus period ( $IST_1$ ), the initial voltage on the capacitor ( $V'_1$ ) is equal to the voltage on the capacitor at the end of the first stimulation period ( $t = ST_1$ ) due to the continuity of voltage, from (7)

$$V'_1 = Rk_1 - Rk_1 \exp(-ST_1/\tau) \quad (15)$$

From the equation for voltage decay during disadaptation (14), the voltage ( $V_2$ ) on the capacitor at the end of the inter-stimulus period ( $IST_1$ ) is:

$$V_2 = Rk_2 \exp(-IST_1/\tau_2) \quad (16)$$

where  $k_2 = V'_1/R$ . This is also the voltage on the capacitor at the beginning of the second stimulation period ( $ST_2$ ). This process is then repeated with each subsequent stimulation period for the complete stimulus train.

This process can be simplified and general equations for voltage and response for  $n$ th-stimulus period in a series of pulse trains can be developed. In general, starting from an initial condition in the first period with the initial voltage on the capacitor equal to zero (an unadapted receptor), we can calculate the voltage and current at any time by the following equations.

In the stimulus period ( $ST_n$ ) of the  $n$ th stimulation (adaptation period):

$$V = Rk_1 - Rk_n \exp(-t/\tau) \quad (\text{group 17})$$

$$I = k_n \exp(-t/\tau) + I_b$$

where

$$k_n = k_1 - V_n/R \quad (n = 1, 3, 5, \dots)$$

$$V_n = Rk'_{n-1} \exp(-IST_n/\tau_2) \quad (\text{at } t = 0)$$

$$I_b = (\tau/\tau_2)(V_{in}/R)$$

$$V'_n = Rk_1 - Rk_n \exp(-ST_n/\tau) \quad (\text{at } t = ST_n)$$

$$k_1 = (\tau/\tau_1)(V_{in}/R) = V_{in}/R - I_b$$

In the inter-stimulus interval ( $IST_n$ ) of the  $n$ th period (disadaptation period):

$$V = V'_n \exp(-t/\tau_2) \quad (\text{group 18})$$

where

$$k'_n = V'_n/R \quad (n = 1, 2, 3, \dots)$$

$$V_{n+2} = Rk_{n+1} \exp(-IST_n/\tau_2) \quad (\text{at } t = IST_n)$$

This series of equations makes it possible to calculate the expected response of the receptor model for any stimulus pulse train (Fig. 2B, Fig. 3B).

### 2.1.5. Response of model to odor plumes

Odor plume time-series were used as environmentally relevant stimuli for our model [21]. These time series data were sampled using a discrete procedure for each 0.1 s sampling period. If the odor stimulation ( $V_{in}$ ) was greater than the remnant voltage ( $V_n$  or  $V_{n+2}$  from group 17), (Eqs. 6, 7, and 15) were used to determine the voltage output. Conversely, if the odor stimulation ( $V_{in}$ ) was equal to or less than the remnant voltage ( $V_n$  or  $V_{n+2}$  from group 18), Eqs. 15 and 16 were used.

### 2.1.6. Data analysis

Data manipulation and analysis were performed by using commercial software packages (Microsoft Excel® or Statistica® for Windows). One-way ANOVAs, post-hoc Tukey-HSD tests, and Pearson's correlation coefficients were calculated using the intensity output of the model and the odor plume data with Statistica® for Windows. Values for  $\tau_1$  and  $\tau_2$  were determined using the pulse response profiles from Gomez et al. [12]. Dr. George Gomez supplied raw neural responses and IVEC (in vivo electrochemistry) data to us. From this, we used total spikes per stimulus from the model and real cells as the neural responses for our fitting procedures. Best-fit values were determined using a maximum likelihood test constructed in Mathematica® for Windows [9]. Both  $\tau_1$  and  $\tau_2$  were allowed to vary simultaneously to produce a three-dimensional likelihood plot. Values for  $\tau_1$  and  $\tau_2$  were chosen

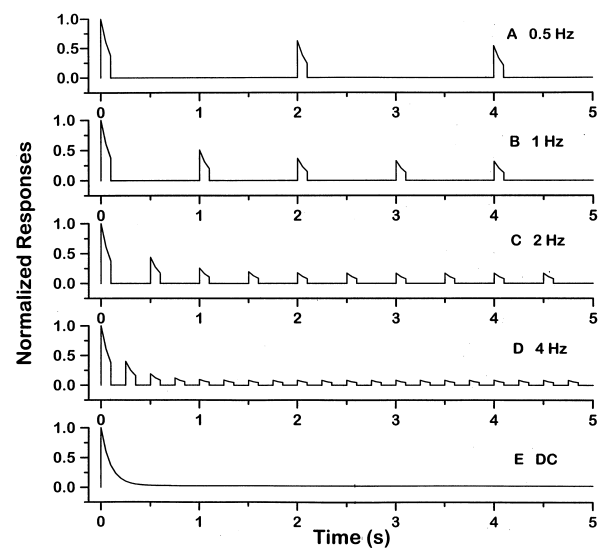


Fig. 3. The response (as current flow) of a model receptor cell to various periodic stimuli with different input frequencies ( $f = 0.5, 1, 2, 4$  Hz) and to a DC step. All model cell responses were normalized to the first stimulation.

that maximized the likelihood for fitting the lobster data. Responses from the model are presented as current ( $I_{out}$ ) per 100 ms. For those analyses that use normalized responses, the maximum response was used to normalize the subsequent responses. Since the stimulation periods lasted 100 ms, we used the total current during that 100 ms epoch for the analysis of periodic stimulation.

### 3. Results

#### 3.1. Fitting of $\tau_1$ and $\tau_2$ to experimental data

To determine the values of  $\tau_1$  and  $\tau_2$  for our model, we have used published neurophysiological data from primary olfactory receptor cells in the lobster, *Homarus americanus* [10,12]. We have chosen these experiments because they represent the only experiments to date in which the stimulus input was measured simultaneously with receptor cell output. The choice of 0.1 and 3.8 s for  $\tau_1$  and  $\tau_2$ , respectively, gave the best fit for the population results from the lobster. Each individual cell will most likely have distinct pairs of values for  $\tau_1$  and  $\tau_2$ , which will give each receptor cell distinct temporal filter properties.

Both pulsatile and turbulent odor simulations were performed using odor signals with a time resolution of 100 ms. Micromolar concentrations within the odor signals were converted directly to volts for the simulations and the output from the model cells was measured as current ( $I_{out}$ ). The intensity of the output current is a relative measure of model cell output and can be related to firing frequency of real receptor cells (No. of spikes per unit time). An increase in current flow of the model cells (as in (Figs. 3, 4, 6, and 7)) can be thought of as an increase in firing frequency of real receptor cells. In the following simulations, ST was always set to 0.1 s for all pulse trains with  $T = 1/f$  (for  $f = 0.5, 1, 2,$  and  $4$  Hz). For the DC stimulation, we set IST = 0.

#### 3.2. Individual and peristimulus responses to repetitive pulses

The response of our model receptor cell to both a series of stimulus trains at different frequencies and to a single DC step stimulus is shown in Fig. 3A–E. Each response was normalized to the maximum response, which always occurs with the initial stimulation. In general, the model receptor cell could faithfully follow pulsatile stimuli up to a frequency of 4 Hz. However, the 4-Hz frequency approached the temporal resolution limit (flicker fusion) for our model receptor cell and the individual responses were weak. It was evident from these series of stimulations that our model cell exhibited two types of adaptation. Within each pulse, the response of the model receptor cell de-

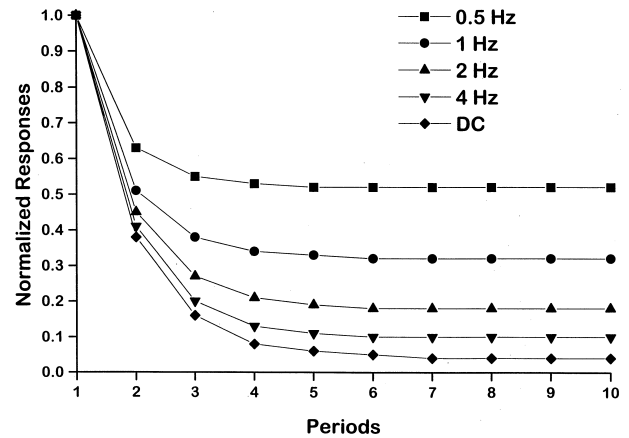


Fig. 4. Cumulative adaptation responses of a model chemoreceptor cell to various periodic stimulus series with frequency  $f = 0.5, 1, 2, 4$  Hz and a DC stimulation. With periodic stimulation, the responses of the model cell drastically decreased to asymptotes after the third response. Responses of the model cells were normalized to the first response. The periods for the DC stimulus were sequential 100 ms bins.

creased despite constant stimulation. In addition, there was a long-term effect of adaptation, which resulted in a lower initial response to each subsequent stimulus pulse (cumulative adaptation; [31]). During adaptation to periodic stimuli or a DC step, the response of the model cell completely adapted after a long time and only the background activity remained ( $I_b$ ). In our model receptor cell and in lobster chemosensory cells, the background activity was very low or completely absent.

#### 3.3. Flicker fusion

Our model receptor cell resolved up to a 4-Hz stimulus frequency (Fig. 3). The response peaked at the initial stimulus pulse and declined to a steady state within 2 s after stimulation began (Fig. 3). This is similar to lobster olfactory cells, which had a peak in response between 100 and 200 ms and a similar decline [12]. Unlike real lobster olfactory cells, our model receptor cells resolved pulsed stimuli faster than 4 Hz. The response magnitude at these higher frequencies is quite small 1–3% of the original response. Given that our model receptor cell has no “noise” associated with its response, we had the ability to resolve these small magnitude responses. If our model receptor cells had a realistic variability and noise that is associated with real receptor cells, our ability to resolve high frequency stimulation would be compromised. In addition, at these higher frequencies, the response magnitude continued to decrease with increasing frequency. The responses failed to fuse after 3 s and remained at a constant level for the remainder of the stimulation period. In contrast, lobster olfactory cells fused in a much shorter time period ( $< 2$  s; [12]).

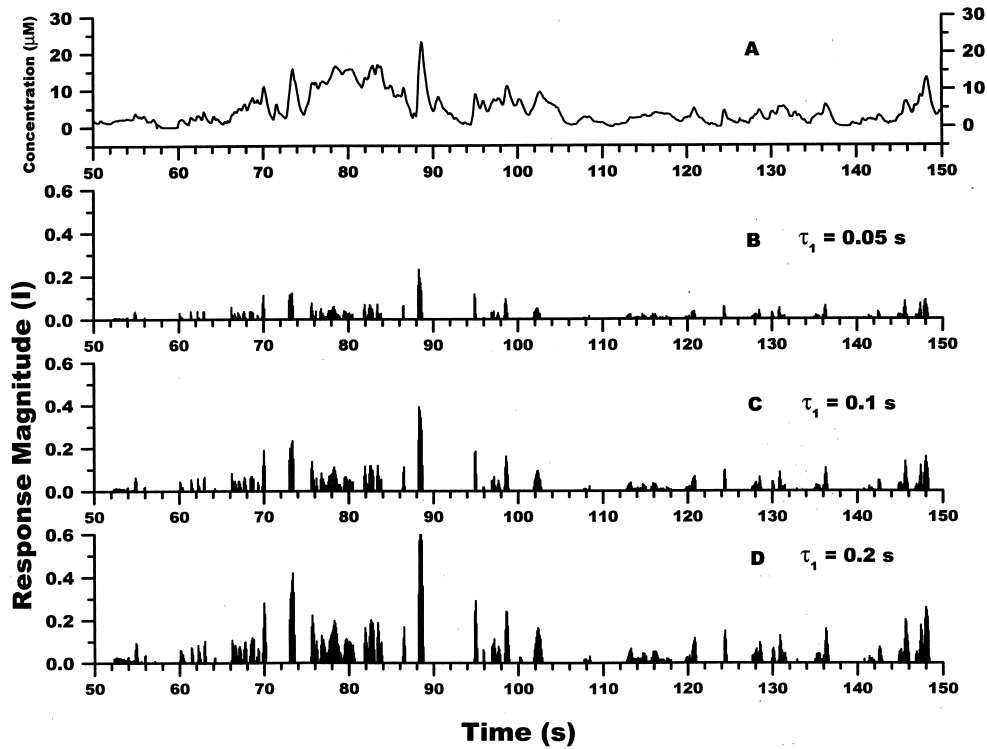


Fig. 5. (A) Stimulus profile of a real turbulent odor plume measured in previous studies [23]. (B–D) Temporal response patterns of model chemoreceptor cells with different  $\tau_1$  values (B = 0.05, C = 0.1, D = 0.2 s). All three model receptor cells had the same  $\tau_2$ , which has been set at 3.8 s. Time constants that match lobster olfactory cells are  $\tau_1 = 0.1$  s and  $\tau_2 = 3.8$  s. In all cases, the value of  $R$  is held constant.

### 3.4. Cumulative adaptation

Repetitive stimulation caused a decrease in the normalized response, which quickly approached an asymptote

after several periods (Fig. 4). The normalized response of the model receptor cell reached this plateau after only three periods for the lower frequencies (0.5 Hz) and after seven periods for the faster frequencies (4 Hz). The great-

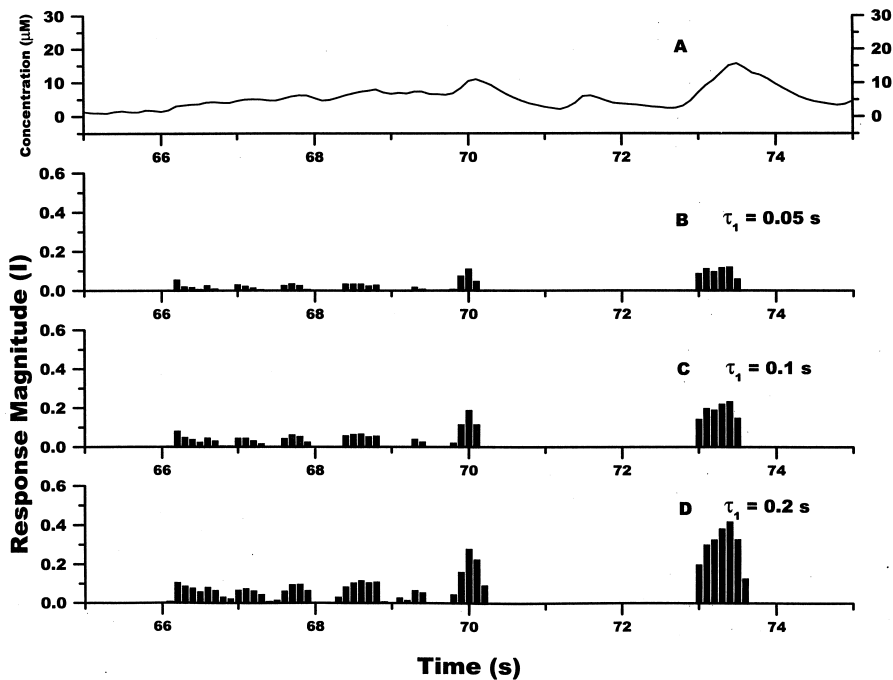


Fig. 6. Enlarged section of this figure showing the time period between 65 and 75 s.

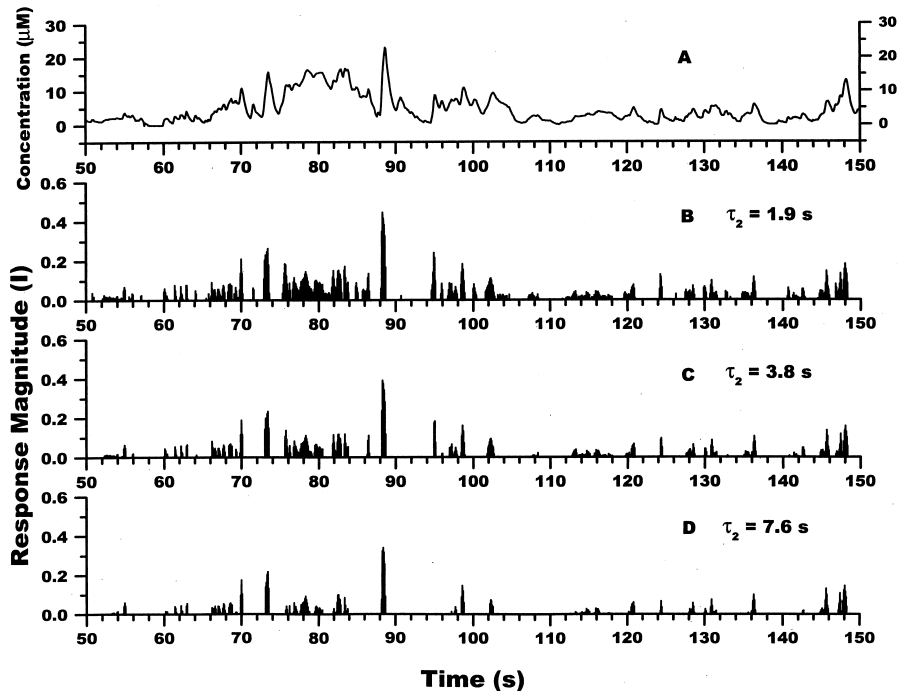


Fig. 7. (A) Stimulus profile of a real turbulent odor plume measured from previous studies [23]. (B–D) Temporal response patterns of model chemoreceptor cells with different  $\tau_2$  values (B = 1.9, C = 3.8, D = 7.6 s). All three model receptor cells had the same  $\tau_1$ , which has been set at 0.1 s. Time constants that match lobster olfactory cells are  $\tau_1 = 0.1$  s and  $\tau_2 = 3.8$  s.

est decrease in response occurred after the first pulse regardless of the stimulation frequency. In addition, the percentage of initial response decreased with increasing frequency.

### 3.5. Response of model cells to turbulent odor signals

To remove any results, which may be biased due to a completely unadapted state of the model receptor cell, all subsequent analyses (on model cell responses to odor signals correlations, response lengths, etc.) were conducted after the first 30 s of odor stimulation. Naturally occurring odor signals are characterized by large fluctuations in intensity over time [19,21]. How model and real receptor cells respond to these concentration fluctuations will depend upon their rates of adaptation and disadaptation. In our model, we could change the two time constants ( $\tau_1$  and  $\tau_2$ ) independently from each other. Fig. 5B–D shows the effect of changing  $\tau_1$  on the response of a model receptor cell. As the first time constant was increased from 0.05 to 0.2 s, the magnitude of response also increased. This was due to the differences in the time dynamics of the model receptor cells, which is the remnant voltage on the capacitor ( $\tau_1 = 0.1$  s fits the data from lobster olfactory cells). For example, with a rapid charging time constant ( $\tau_1 = 0.05$  s), the threshold of the model receptor cell increased almost as quickly as the rate of stimulus concentration increased during an odor pulse. The difference

between the stimulus concentration and the concentration that was above the remnant voltage of the receptor cell remained small (Fig. 5, e.g.,  $t = 88$  s). Conversely, with a slower charging time constant, the concentration within an odor pulse increased at a faster rate than the increase in the remnant voltage, the model receptor cell responses were greater in magnitude. In addition, this rate had a significant effect on the length of response. (Length of response is measured as the time of current flow of a response and is surrounding at the start and finish by zero current flow periods.) The average length of the responses were 0.37, 0.49, and 0.69 s for  $\tau_1 = 0.05$ , 0.1, and 0.2 s, respectively. These differences were significant ( $p < 0.05$ , Tukey-HSD test). The model receptor cell with the faster rate of adaptation resolved the stimulus fluctuations into smaller and more discrete pulses (Fig. 6, e.g.,  $t = 66$ –70 s). During this period of odor stimulation, the rapidly adapting cell and intermediate cell encodes six discrete odor pulses (Fig. 6B and C). The slowest adapting cell encodes only three distinct pulses (Fig. 6D). (Pulses are considered distinct when a period of zero current flow occurs between them). Also, note the changes in magnitude of current flow between the three cells at 70 s. Regardless of the time constants and corresponding rates of adaptation or disadaptation, the responses from all of the model cells to a turbulent odor plume were characterized by short, intermittent periods of current flow. Prolonged current flow from any of the cells was missing. Changes in disadaptation

time constant did not have a significant effect on response length.

In addition, the magnitude of current flow in the receptor cells was significantly correlated to the concentration level of the stimulus input (Fig. 5, e.g.,  $t = 72\text{--}82$  s,  $r^2 = 0.16, 0.21,$  and  $0.30$  for  $\tau_1 = 0.05, 0.1,$  and  $0.2$  s, respectively,  $p < 0.05$ ). Although the correlation of response with odor plume concentration was weak for all three adaptation times, the correlation was stronger as the adaptation time constant was lengthened. This relationship was also seen for changes in the disadaptation time constant, but the correlation weakened as the disadaptation time constant was lengthened. In addition, the correlation coefficients were less sensitive to changes in the disadaptation time constant.

Changes in the second time constant ( $\tau_2$ ) also affected the response of the model cell. As  $\tau_2$  is increased from 1.9 to 7.6 s, the response of the model receptor cell decreased (Fig. 7B–D;  $\tau_2 = 3.8$  s fits data from lobster olfactory cells). Model receptor cells with rapid disadaptation time courses recovered from a previous high concentration quickly allowing them to respond fully to the next stimu-

lus. Model receptor cells with long disadaptation time constants remained adapted and could not resolve small odor pulses that follow a large concentration pulse (Fig. 7D; e.g.,  $t = 95\text{--}100$  s). Conversely, model receptor cells with rapid disadaptation rates resolved more pulses within a succession of odor stimuli (Fig. 7B; e.g.,  $t = 95\text{--}100$  s). It was clear from these changes in the two time constants that  $\tau_2$  affected the ability of a model receptor cell to encode pulse series while  $\tau_1$  affected the ability of a model receptor cell to encode series pulses and the magnitude of concentration within a single odor pulse. These model responses were similar in regard to reduced magnitude and temporal structure to responses from lobster olfactory neurons to turbulent odor presentations (Fig. 8A and B). The responses presented in this figure are single olfactory neurons responding to fluctuations in concentration of hydroxy-proline. The tracer chemical (dopamine) was mixed in with the olfactory stimulus, hydroxy-proline, and concentrations of dopamine were measured simultaneously with the neural output. For details on these simultaneous recording techniques and neurophysiological methods, see [11,12].

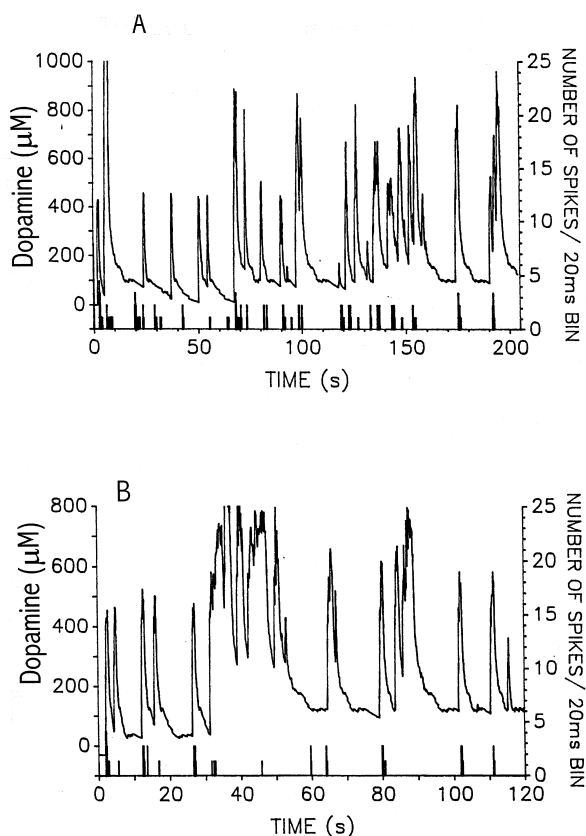


Fig. 8. Stimulus profile of turbulent odor presentations within a neurophysiological recording chamber (left-hand axis) and the simultaneously recorded neural output of lobster olfactory cells (right-hand axis). A and B are different receptor cells. Neural output is measured as the number of action potentials per 20 ms bin. For more details regarding the recording and measuring of neural signals from lobster olfactory cells, see [11,12].

#### 4. Discussion

Physiological models can play an important role in understanding the mechanisms by which sensory systems extract information from environmental signals. This is especially true for chemosensory systems due to the turbulent and chaotic structure of environmental odor signals. It is extremely difficult to mimic turbulent odor signals in neurophysiological recording chambers and impossible to present the same turbulent odor signal to different receptor cells. Models can provide a means of presenting identical stimuli to receptor cells with different physiological properties, which permits some insight into the filtering of realistic odor signals. This is true only if the physiological models have assumptions based on real electrophysiological data from actual receptor cells.

Our model cells responded analogously to real receptor cells under identical stimulation conditions. When presented with a train of odor pulses, our model cells exhibited two forms of adaptation (Fig. 3). First, within a single pulse, the response decreases despite prolonged stimulation. Second, the response decreased with subsequent stimulation in the pulse train and the magnitude of decrease was dependent upon the stimulation frequency (cumulative adaptation; [31]). The rate of cumulative adaptation for our model cells mimics that found in real receptor cells [12]. When presented with turbulent odor profiles, model cells responded to stimulus pulses with very short bursts of current (Figs. 5–7). Since the response to any single odor stimulation was dependent upon a number of factors including previous concentrations, current concentration and

the two physiological time constants, changes in the time constants had a profound influence on the output of the model receptor cell. Increases in  $\tau_1$  (adaptation time constant) served to increase the response of the model cell (Fig. 5; e.g.,  $t = 88$  s).

This can be explained by how  $\tau_1$  affects the threshold of the model receptor cell. In our model, we simulate the receptor cell adaptation by raising the threshold (capacitor voltage) of the model receptor cell. For very small values of  $\tau_1$ , the threshold of the model receptor cell changes very quickly to the raising concentration and the difference between the stimulus concentration and the threshold level remains small. Conversely, for large values of  $\tau_1$ , the threshold of the model receptor cell responds slowly to the rising stimulus level and the difference between stimulus and cell threshold remains large. The response of this model cell is larger than a model cell with a small  $\tau_1$ . This is only apparent when stimulus pulses are presented as ramps or slopes and is not present for square-wave stimulation. Identical findings with ramped stimuli were presented elsewhere [19].

All environmentally relevant stimuli have a slope. The ability of receptor cells to respond differently to different slopes is important for translating concentration–response functions derived under assumed square-wave (or unmeasured waveform) stimulation in physiological chambers to the concentration–response properties of the system under realistic stimulation. Previous models serve to show that the adaptation time constants determine the receptor cells' sensitivity to slope of the stimulus, but did not reveal changes in concentration–response functions [19,20].

Changes in the second time constant,  $\tau_2$ , had two consequences for the response of the model receptor cell. First, short time constants, e.g.,  $\tau_2 = 1.9$  s, increased the response of the model cell but to a much smaller degree than changes in  $\tau_1$ . More importantly, changes in  $\tau_2$  influenced the ability of the model cell to resolve odor fluctuations into discrete pulses. Model receptor cells with smaller values for  $\tau_2$  resolved more of the small-scale concentration fluctuations within odor signals (Fig. 7). Although the true disadaptation time constant of the model cell incorporates both  $\tau_1$  and  $\tau_2$ , it is  $\tau_2$  that is more important for the temporal resolution of the cell. For instance, if a large concentration peak occurs before a series of smaller concentrations, model cells with long recovery times will not respond to the smaller fluctuations (Fig. 7D; e.g.,  $t = 88$ – $100$  s). Conversely, model cells with quick recovery times will respond to many of the smaller stimulus fluctuations.

The two time constants of our model define both the temporal filtering capabilities and the dynamic concentration–response function of receptor cells. A receptor cell with these physiological properties becomes a temporal filter for incoming dynamic signals (Fig. 8). Different time constants bestow upon a receptor cell a concentration–frequency specific response profile. Receptor cells with

shorter adaptation and disadaptation time constants will respond greater to shorter periods of stimulation and are able to follow higher frequency stimulation. Conversely, receptor cells with longer adaptation and disadaptation time constants will respond greater to a lower frequency of odor stimulation. This type of signal analysis may be important for those animals that use purely chemical information to orient to chemical sources.

It has been shown in other sensory systems that physiological filters are 'matched' to the dominant stimulus properties [32]. Other studies have suggested that the frequency filter properties of chemoreceptor cells are matched to the dominant frequencies within biologically relevant turbulence [3,20]. The dominant frequencies in aquatic odor plumes which have been quantified are below 4 Hz [21,23], while the dominant frequencies in aerial plumes appear to be much higher (10–30 Hz; [24,25]). In fact, peripheral and CNS neurons of insects can resolve faster stimulus fluctuations (up to 10 Hz; [6,14,26]) than lobster olfactory neurons (up to 4 Hz; [11]). We find that the time constants derived from aquatic physiological studies give maximal responses to stimulus frequencies at or below 4 Hz. Other chemoreceptor systems under different environmental constraints will most likely have different physiological time constants to maximize response profiles to different stimulus conditions.

As a consequence of the dynamic structure of odor signals and the temporal properties of our model receptor cells, the encoding of stimulus properties may be different than what has been proposed previously. It has been suggested that chemoreceptor cells are not responding to concentration but instead measure concentration per unit time. Chemoreceptor cells are actually flux detectors or concentration detectors [13]. Similarly, our model shows that absolute concentration as a single stimulus parameter has become decoupled from the magnitude of model cell response. However, our analysis shows that our model receptor cells are responding to the derivative of the flux or rate of concentration change per unit time. For example, the concentration peaks located at 73, 79, 80, and 83 s (Fig. 5) are nearly identical in amplitude. Each of our model receptor cells responds differently to each of these stimulus concentrations. The magnitude of response is dependent not only on the current stimulus concentration, but also on the previous stimulus concentration. Similar examples are found throughout the time series shown in Figs. 5 and 7. This change in model receptor cell property is important when considering how intensity information is encoded by chemosensory systems. Our model suggests that the physiological mechanisms underlying adaptation and disadaptation is one of the mechanisms that differentiate cells into flux detectors or concentration detectors (as defined by [13]). This is also seen in the neurophysiological data presented here (Fig. 8).

In summary, this model shows that the temporal properties of chemoreceptor cells can be modeled using a simple

electrical circuit with two time constants. This model shows that changes in these time constants can have dramatic effects on how individual cells encode both intensity and temporal information contained within odor signals. In addition, this model also points to certain areas that need further investigation. These include how different rates of adaptation and disadaptation influence the ability of cells to encode both the quality and quantity of chemical signals, what cellular events influence the intrinsic time constants of receptor cells, and what important features of turbulent plumes are passed on to higher order neurons.

## Acknowledgements

The authors would like to thank Drs. Jelle Atema, George Gomez, and Rainer Voigt for supplying us with the neurophysiological data on which this model is based. The authors would particularly like to thank Dr. Rainer Voigt for collecting the neural data presented in Fig. 8. We would also like to thank Drs. Stan Smith, George Gomez, and Chuck Derby for critically reviewing this manuscript and Dr. Adam Porter for likelihood statistical analysis. This research is supported by NSF grant OCE-9496270. Contribution number 2 from the Center for Neuroscience, Mind and Behavior.

## References

- [1] B.W. Ache, Integration of chemosensory information in aquatic invertebrates, in: J. Atema, A.N. Popper, R.R. Fay, W.N. Travalga (Eds.), *Sensory Biology of Aquatic Animals*, Springer-Verlag, New York, 1988, pp. 387–401.
- [2] T.J. Almaas, T.A. Christensen, H. Mustaparta, Chemical communication in heliothine moths: I. Antennal receptor neurons encode several features of intra- and interspecific odorants in the male corn earworm moth *Helioverpa zea*, *J. Comp. Physiol. A.* 169 (1991) 249–258.
- [3] J. Atema, Distribution of chemical stimuli, in: J. Atema, A.N. Popper, R.R. Fay, W.N. Travalga (Eds.), *Sensory Biology of Aquatic Animals*, Springer-Verlag, New York, 1988, pp. 29–56.
- [4] T.C. Baker, M.A. Willis, K.F. Haynes, P.L. Phelan, A pulsed cloud of pheromone elicits upwind flight in male moths, *Physiol. Entomol.* 10 (1985) 257–265.
- [5] P.F. Borroni, J. Atema, Adaptation in chemoreceptor cells: I. Self-adapting backgrounds determine threshold and cause parallel shifts of response function, *J. Comp. Physiol. A.* 164 (1988) 67–74.
- [6] T.A. Christensen, J.G. Hildebrand, Frequency coding by central olfactory neurons in the sphinx moth *Manduca Sexta*, *Chem. Senses* 13 (1988) 23–130.
- [7] D.R. Curtis, J.C. Eccles, Synaptic action during and after repetitive stimulation, *J. Physiol.* 150 (1960) 374–398.
- [8] J.C. Eccles, *The Physiology of Nerve Cells*, Johns Hopkins Univ. Press, 1957.
- [9] A.W.F. Edwards, *Likelihood: Expanded Edition*, Johns Hopkins Univ. Press, 1992.
- [10] G. Gomez, J. Atema, Time course of recovery from adaptation by hydroxyproline-sensitive lobster olfactory receptors, *Biol. Bull.* 187 (1994) 259–260.
- [11] G. Gomez, R. Voigt, J. Atema, High resolution measurement and control of chemical stimuli in the lateral antennule of the lobster *Homarus americanus*, *Biol. Bull.* 183 (1992) 353–354.
- [12] G. Gomez, R. Voigt, J. Atema, Frequency filter properties of lobster chemoreceptor cells determined with high-resolution stimulus measurement, *J. Comp. Physiol. A.* 174 (1994) 803–811.
- [13] K.E. Kaissling, Flux detectors versus concentration detectors: two types of chemoreceptors, *Chem. Senses* 23 (1998) 99–111.
- [14] K.E. Kaissling, C. Zack-Straussfeld, E. Rumbo, Adaptation processes in insect olfactory receptors: mechanisms and behavioral significance, in: S. Roper, J. Atema (Eds.), *Olfaction and Taste IX*, N. Y. Acad. Sci., 1987, pp. 104–112.
- [15] J.S. Kennedy, A.R. Ludlow, C.J. Sanders, Guidance of flying male moths by wind-borne sex pheromone, *Physiol. Entomol.* 6 (1981) 395–412.
- [16] L. Lapique, Recherches quantitatives sur l'excitation électrique des nerfs traitée comme une polarisation, *J. Physiol. Pathol. Gen.* 9 (1907) 620–635.
- [17] A. Mafrá-Neto, R.T. Cardé, Fine-scale structure of pheromone plumes modulates upwind orientation of flying moths, *Nature* 369 (1994) 142–144.
- [18] W.C. Michel, B.W. Ache, Odor-activated K<sup>+</sup>-conductance inhibits lobster olfactory receptor cells, *Chem. Senses* 15 (1991) 619–620.
- [19] P.A. Moore, A model of the role of adaptation and disadaptation in olfactory receptor neurons: implications for the coding of temporal and intensity patterns of odor signals, *Chem. Senses* 19 (1994) 71–86.
- [20] P.A. Moore, J. Atema, A model of a temporal filter in chemoreception to extract directional information from a turbulent odor plume, *Biol. Bull.* 174 (1988) 355–363.
- [21] P.A. Moore, J. Atema, Spatial information in the three-dimensional fine structure of an aquatic odor plume, *Biol. Bull.* 181 (1991) 408–418.
- [22] P.A. Moore, N. Scholz, J. Atema, Chemical orientation of lobsters, *Homarus americanus*, in turbulent odor plumes, *J. Chem. Ecol.* 17 (1991) 1293–1307.
- [23] P.A. Moore, R.K. Zimmer-Faust, S.L. BeMent, M.J. Weissburg, J.M. Parrish, G.A. Gerhardt, Measurement of microscale patchiness in a turbulent aquatic odor plume using a semiconductor-based microprobe, *Biol. Bull.* 183 (1992) 138–143.
- [24] J. Murlis, C.D. Jones, Fine-scale structure of odour plumes in relation to insect orientation to distant pheromone and other attractant sources, *Physiol. Entomol.* 6 (1981) 71–86.
- [25] J. Murlis, M.A. Willis, R.T. Cardé, Odor signals: patterns in space and time, in: K. Døving (Ed.), *Proceedings of the Tenth International Symposium on Olfaction and Taste*, Graphic Communication System, Oslo, 1991, pp. 6–17.
- [26] E.R. Rumbo, K.E. Kaissling, Temporal resolution of odor pulses by three types of pheromone receptor cells in *Antheraea polyphemus*, *J. Comp. Physiol. A.* 165 (1989) 281–291.
- [27] R.J. Tocci, *Fundamentals of Pulse and Digital Circuits*, Charles E. Merrill Publishing, Columbus, OH, 1972.
- [28] H.C. Tuckwell, *Introduction to Theoretical Neurobiology, Linear Cable Theory and Dendritic Structure Vol. 1* Cambridge Univ. Press, Oxford, 1988.
- [29] N.J. Vickers, T.C. Baker, Male *Heliothis virescens* maintain upwind flight in response to experimentally pulsed filaments of their sex pheromone (*Lepidoptera: Noctuidae*), *J. Insect. Behav.* 5 (1992) 669–687.
- [30] N.J. Vickers, T.C. Baker, Reiterative responses to single strands of odor promote sustained upwind flight and odor source location by moths, *PNAS* 91 (1994) 5756–5760.

- [31] R. Voigt, J. Atema, Adaptation in chemoreceptor cells: III. Effects of cumulative adaptation, *J. Comp. Physiol. A.* 166 (1990) 865–874.
- [32] R. Wehner, 'Matched filters' — neural models of the external world, *J. Comp. Physiol. A.* 161 (1987) 511–531.
- [33] M.J. Weissburg, R.K. Zimmer-Faust, Odor plumes and how blue crabs use them in finding prey, *J. Exp. Biol.* 197 (1994) 349–375.
- [34] H. Westerberg, Properties of aquatic odour trails, in: K. Døving (Ed.), *Proceedings of the Tenth International Symposium on Olfaction and Taste*, Graphic Communication System, Oslo, 1991, pp. 45–65.